Hindawi Publishing Corporation
International Journal of Photoenergy
Volume 2012, Article ID 536194, 8 pages
doi:10.1155/2012/536194

Research Article

Preparation and Characterization of $(I_2)_n$ Sensitized Nanoporous TiO_2 with Enhanced Photocatalytic Activity under Visible-Light Irradiation

Juzheng Zhang,[1] Xin Liu,[1] Shanmin Gao,[1,2] Quanwen Liu,[1] Baibiao Huang,[2] and Ying Dai[2]

[1] *School of Chemistry and Materials Science, Ludong University, Yantai 264025, China*
[2] *State key labs of Crystal Materials, Shandong University, Jinan 250100, China*

Correspondence should be addressed to Shanmin Gao, gaosm@ustc.edu and Baibiao Huang, bbhuang@sdu.edu.cn

Received 18 December 2011; Accepted 31 January 2012

Academic Editor: Xuxu Wang

A yellow/brown powder of $(I_2)_n$ sensitized nanoporous TiO_2 was obtained via an hydrolysis with $TiCl_4$ and iodine hydrosol as raw material. I_2 nanoparticles in the hydrosol were used as seeds to initiate the nucleation of a precursory TiO_2 shell. The hybridized jumbles were further calcinated at different temperatures. The structure, crystallinity, morphology, and other physical-chemical properties of the samples are characterized by X-ray diffraction (XRD), transmission electron microscopy (TEM), N_2 adsorption-desorption isotherms measurements, and UV-vis diffuse reflectance spectroscopy (DRS). The formation mechanism of these $(I_2)_n$ sensitized nanoporous TiO_2 is discussed. Methylene blue solutions were used as model wastewater to evaluate the visible light photocatalytic activity of the samples. The results indicate that iodine can exist even in high-temperature calcination for iodine being encapsulated in the nanocavities inside TiO_2. The degradation of methylene blue (MB) accorded with the first-order reaction model.

1. Introduction

Semiconductor-catalyzed photooxidation using solar light as an energy source is one of the most efficient processes for a rapid and low-cost degradation of organic pollutants. The excellent chemical stability, nontoxicity, and photoactivity of TiO_2 has attracted much attention for its potential use as a solid photocatalyst for environmental purification [1–3]. However, because of its large bandgap of 3.20 eV, only a small UV fraction of solar light, about 2-3%, can be utilized to generate electron-hole pairs. Hence, it is crucial to enhance the light harvesting of TiO_2 in the visible region which accounts for more than 43% of the total solar energy [4, 5].

In general, two methods are utilized to enhance the light harvest of TiO_2 in the visible region. One method is to sensitize TiO_2 with color centers that have proper energy levels for photoelectron transfer between the color centers and TiO_2. A cost-effective sensitization of TiO_2 is typically achieved by adding nonmetals such as I_2 [6–8] and S [9, 10]. The other way is to form a doping level through intercalation of proper atoms into anatase form. For example, by doping carbon [11, 12] and nitrogen [13–15] atoms into the TiO_2 lattice, a new, weak absorption is generated at lower energies and promising approach for inducing effective Vis-absorption.

In addition to the narrow bandgap, the enhancement of surface area of the TiO_2 is another important aspect for the efficiency of the materials because the desired photocatalytic reactions occur at the interfaces of the catalyst-pollute solution [16, 17]. Mesoporous TiO_2 with high specific surface area can provide abundant active sites to adsorb reactant molecules and facilitate the accessibility of reactants to the catalysts [18, 19]. Light efficiency can also be enhanced due to the increased specific surface area and multiple scattering [20].

As a photosensitizer, element iodine not only has the absorption ability in the visible light region but also has low toxicity and can be dissolved in many solvent. Therefore, the elemental iodine can be used as a photosensitizer and prepared visible light photocatalytic materials. Titanium(IV)

alkoxides have been frequently studied as titanium precursors, but their high cost and the need to handle organic solvents are important drawbacks. Inorganic precursors are preferable, and TiO_2 powders have been often prepared by hydrolysis of $TiCl_4$, generally in aqueous acidic solutions [21] and in pure water [22, 23].

Based on the above state-of-the-art designing strategies for TiO_2-based photocatalysts, this paper reports the synthesis of high surface area $(I_2)_n$ sensitized nanoporous TiO_2. The I_2 sensitized is confined preferentially in the surface/near surface region of TiO_2 structure in order to accommodate hot carriers in the surface region. The I_2 nanoparticles in the I_2-hydrosol serve as seeds for nucleation of small TiO_2 particles formed from the hydrolysis of the $TiCl_4$. This template-free soft synthetic strategy allows the doping and pore formation to be accomplished simultaneously during calcination, while the amount and position of doping elements can be readily controlled under mild conditions.

2. Experimental

2.1. Materials and Sample Preparation. All chemicals used in this study were reagent grade (Tianjin Ruijinte Chemical Reagent Corp.) without further purification. Water used was deionized and doubly distilled. The $(I_2)_n$ sensitized porous TiO_2 samples were synthesized via the hydrolysis of $TiCl_4$ in iodine hydrosol without using any templates or surfactants, followed by calcination at elevated temperatures.

A typical procedure for preparing the samples is described as follows. First, 0.80 g iodine powders were dissolved in 40 mL absolute ethanol and slowly added dropwisely into 100 mL of distilled water at 60°C with continuous stirring. The I_2 hydrosol was formed after stirring for 0.5 h and then cooled to room temperature. 8 mL $TiCl_4$ was carefully added into 40 mL-deionized water with gentle stirring in ice-water bath to avoid a drastic hydrolysis of $TiCl_4$ in water (designated solution A). Solution A was then added dropwise with vigorous stirring into 100 mL of I_2 hydrosol at room temperature, then the mixture solution was heated to 40°C and keet for 2 h under closed conditions. After that, a 20% (w/w) solution of ammonia was added dropwise with vigorous stirring until pH = 7, then the mixed solution was cooled down to room temperature and aged further to precipitate growth. Finally, the precipitates were centrifuged, washed with distilled water three times, and dried in an oven at 50°C. The precipitates obtained were calcined at different temperatures in air for 3 h. The samples after heat treatment were denoted as IT-T, where the second T indicates the calcination temperatures (in °C). In addition, commercial P25 (~80% anatase and ~20% rutile, Deguass) was used as a reference.

2.2. Characterization. The phases of the final products were identified using X-ray diffractometer (XRD) (Rigaku D/max-2500VPC) with a Ni-filtered Cu Kα radiation at a scanning rate of 0.02° s^{-1} from 20° to 70°. The morphology of the samples was observed with transmission electron microscope (TEM, Hitachi model H800) using an accelerating voltage of 100 kV. Ultraviolet-visible (UV-vis) diffuse reflection spectra (DRS) were recorded in the range 200–800 nm at room temperature (Shimadzu UV-2550 UV-vis spectrophotometer). Porous structure and BET surface area were characterized by an N_2 adsorption-desorption isotherm (ASAP-2020 Micromeritics Co.). Note that the samples were degassed at 180°C prior to the BET measurements. The pore volume and pore diameter distribution were derived from desorption branches of the isotherms by the Barrett-Joyner-Halenda (BJH) model. The BET surface area was calculated from the linear part of the Brunauer-Emmett-Teller (BET) plot.

2.3. Adsorption and Photocatalytic Activity Measurements. The adsorption capability and visible light photocatalytic activity of the $(I_2)_n$ sensitized porous TiO_2 were evaluated by measuring the adsorption and decomposition rate of methylene blue (MB) solution at room temperature. For comparison, the same measurements were also performed on the commercial P25. For a typical absorption and photocatalytic experiment, a total of a 200 mg sample was added to 150 mL MB aqueous solution (5.0×10^{-4} mol/L) in a custom-made quartz reactor. The MB concentration was monitored by the UV-vis spectroscopy during the entire experiment. The solution was irradiated by visible light supplied by a 300 W tungsten-arc lamp (Zhejiang Electric Co. Ltd.) with a glass filter (transparent for $\lambda > 400$ nm). After 5 minute intervals during adsorption and visible light illumination, about 3 mL aliquots were taken out and centrifuged to remove the trace particles. The absorbance of the centrifuged solution was measured in the range 500–800 nm using a UV-vis spectrophotometer (Shimadzu UV-2550).

3. Results and Discussions

3.1. Sample Structure. The porous nanostructures were prepared via the hydrolysis of $TiCl_4$ in I_2 hydrosol, followed by calcinated in air at elevated temperatures for 3 h. Powder X-ray diffraction (PXRD) is used to investigate the changes of structure and crystallite sizes of the prepared porous samples at different calcination temperatures. Figure 1 shows the XRD patterns of the samples after being calcinated at various temperatures from 200°C to 600°C. The XRD pattern for the sample obtained at 200°C indicated the sample predominantly amorphous titania besides trace amounts of anatase. The diffraction peaks at $2\theta = 31.6°$, 33.5° and 36.0° should be the iodine (JCPDS no. 71-1370). As the calcination temperatures increase, the XRD results show the pure anatase TiO_2 phase (JCPDS file no. 21-172), indicating that the crystallization of the samples is achieved. In addition, as the calcination temperature increases, the peaks assigned to anatase become sharper and more intense due to the formation of larger grains as summarized in Table 1. The average crystallite sizes of $(I_2)_n$ sensitized nanoporous TiO_2 are 4.1, 7.2, 9.8, and 13.2 nm for IT-300, IT-400, IT-500, and IT-600, respectively, which are estimated from the full width

Table 1: Physicochemical properties of IT-T samples from N_2 sorption analysis and XRD results.[a]

Sample	S_{BET} (m^2/g)	Pore volume (cm^3/g)	Average pore size (nm)	Crystal size (nm)
IT-200	508.04	1.287	9.863	
IT-300	287.10	0.241	3.634	4.1
IT-400	247.64	0.180	16.350	7.2
IT-500	175.02	0.152	20.071	9.8
IT-600	163.71	0.148	26.851	13.2

[a] BET surface areas were calculated from the linear part of the BET plots. Total pore volumes were obtained from the volume of N_2 adsorbed at $P/P_0 = 0.995$ Average pore diameters were estimated using the desorption branch of the isotherm and the Battett-joyner-Halenda (BJH) formula. Crystal size was determined by XRD using Scherrer equation.

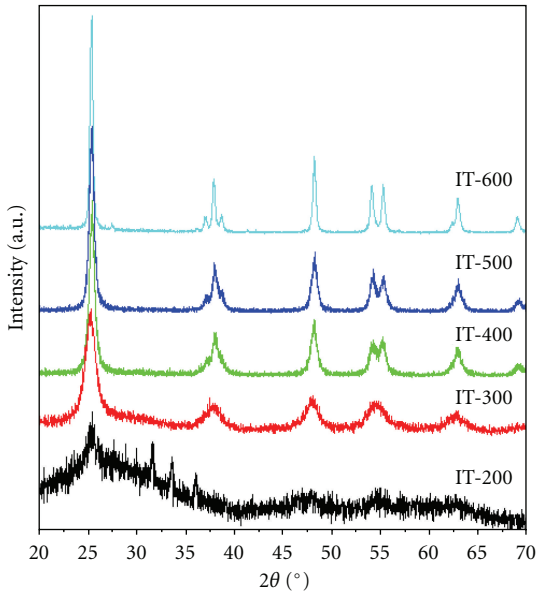

Figure 1: XRD patterns of the corresponding $(I_2)_n$ sensitized IT-T samples after calcinated at 200°C, 300°C, 400°C, 500°C, and 600°C.

at half maximum of the diffraction peak using the Scherrer equation.

Figure 2 shows the TEM images of IT-T samples before and after being calcinated at different temperatures. The average particle size of the precursor is estimated to be 21 nm, as presented in Figure 2(a). No porous structure was observed at this point. The wormhole-like irregular mesopores for $(I_2)_n$ sensitized porous TiO_2 can be observed in Figures 2(c)–2(f). The sample obtained at 200°C shows the noncrystalline nature of amorphous (Figure 2(b)), but there were porous structure. The amorphous structure is consistent with the XRD result, and the porous structure is caused by the I_2 and H_2O gas escape at heat treatment process. It is the subsequent heat treatment that creates the mesoporous structures. The apparent common feature of the four samples after heat treatment at 300°C, 400°C, 500°C and 600°C is that they all consist of pseudospherical TiO_2 particles. Furthermore, each individual sphere is composed of a large number of much smaller and loosely packed TiO_2 nanoparticles (about 4~10 nanometers in diameter). As a result, the interstitial voids among these primary nanoparticles constitute a short-range disordered nanoporous structure. We also notice that the size of the primary nanoparticles grows with the increasing calcination temperature.

Pore size and specific surface area of the as-prepared samples were characterized by nitrogen adsorption-desorption isotherm measurements. Figure 3 shows the results obtained from N_2 adsorption-desorption isotherm studies and analyzed by BET method for surface area and BJH pore size distribution. The surface area and porosity have been measured for all of the IT-T samples, and the results are given in Table 1. Calcination treatment showed a significant influence on the isotherm behavior of the samples. The VI-type isotherms for sample IT-200 and IV like Isotherm for samples IT-300, IT-400, IT-500, and IT-600 shown in Figure 3(a) demonstrate typical characteristics of mesoporous structure in the materials [24]. From the isotherms, it can be seen that the monolayer adsorption is complete when the relative pressure reaches 0.7 for sample IT-600. However, the monolayer adsorption for other samples is not complete until reaching a relative pressure of 0.8 for sample IT-300 and 0.78 for IT-400. This indicates that sample IT-600 possesses much smaller pore size than other samples. Although mesopores contribution could be observed in Figure 3(b) for IT-600, overall pore volume measured is 0.148 cm^3g^{-1}, indicating that the contribution from mesoporous is small. Less mesoporosity in IT-600 may be attributed to the large size of the particles. This result agrees with the XRD and TEM results.

Table 1 summarizes the BET-specific surface area and the apparent average pore size of our samples. The pore volume and specific surface area decrease with increasing calcination temperature. However, the samples still maintain relatively high specific surface area and pore size even for sample IT-600, which is calcined at 600°C. Consequently, this may enhance catalytic activity, as demonstrated later in the measurement of photocatalytic activity on degradation of methylene blue.

3.2. Possible Formation Mechanism of $(I_2)_n$ Sensitized Nanoporous TiO_2. Different from the conventional doping method, in which the iodine (or its precursors) is added to the matrix of TiO_2, we adopt a counter strategy to add precursors

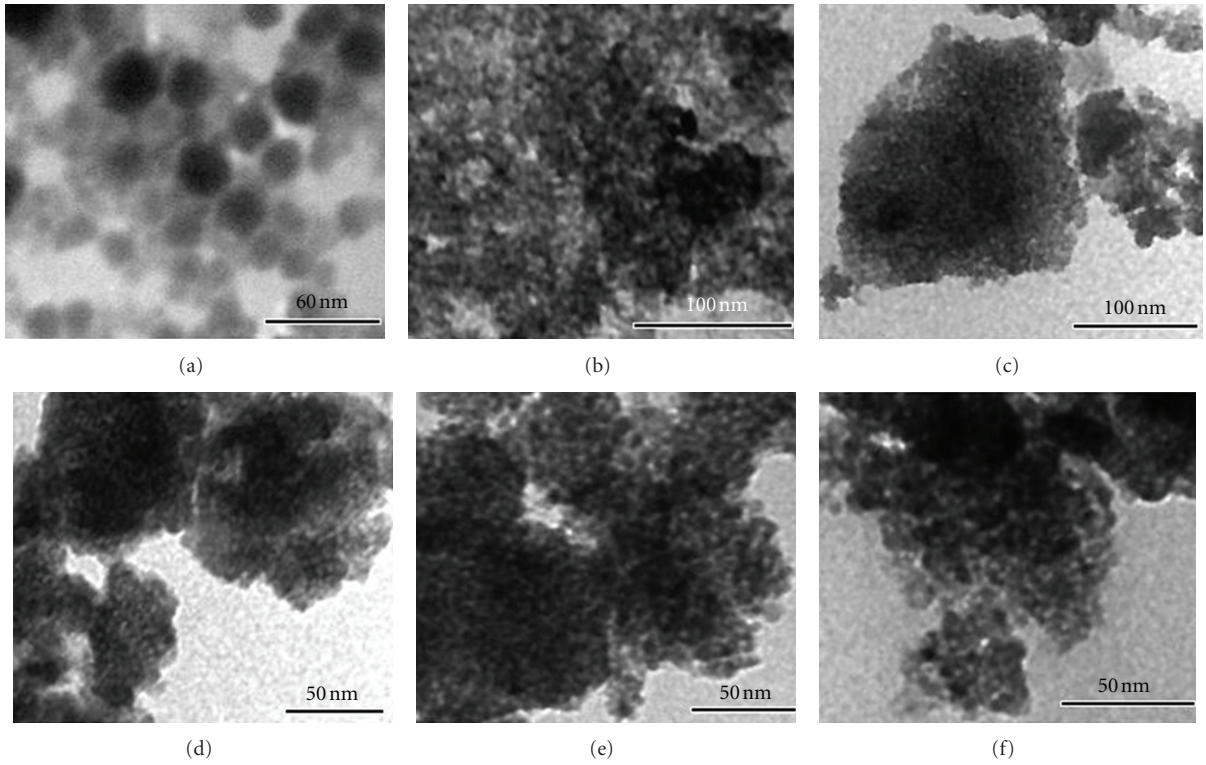

Figure 2: TEM images of the precursor of $(I_2)_n$-sensitized nanoporous TiO_2 (a), and IT-T calcined for 3 h at (b) 200°C; (c) 300°C; (d) 400°C, (e) 500°C and (f) 600°C.

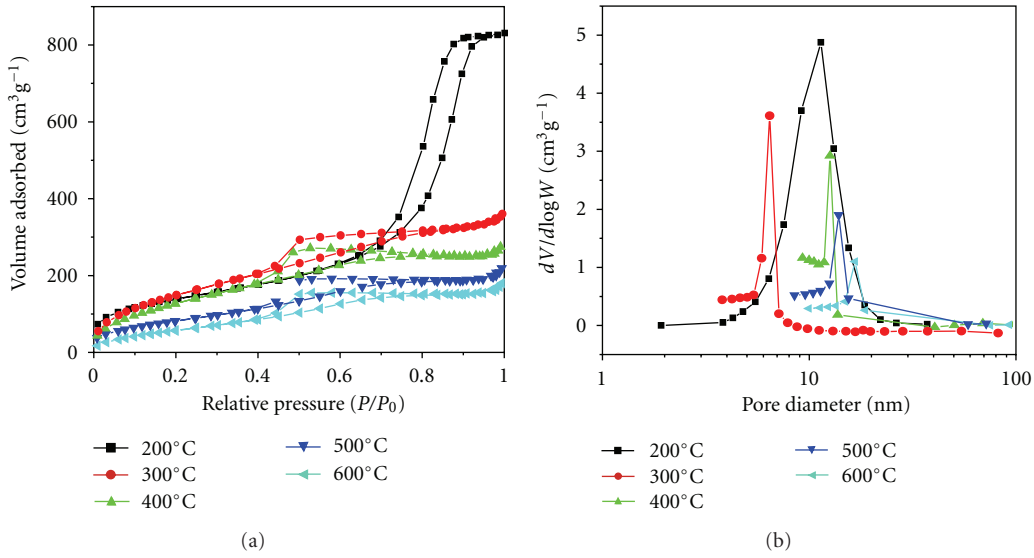

Figure 3: N_2 adsorption/desorption isotherms (a) and the corresponding BJH pore size distributions (b) of the as-prepared IT-T samples.

of TiO_2 into the matrix of I_2 nanoparticles formed in the I_2 hydrosol. A possible multistep mechanism, illustrated in Figure 4, is proposed to interpret the formation of the $(I_2)_n$ sensitized nanoporous TiO_2. When $TiCl_4$ solution was added to I_2 hydrosol, the heat of the exothermic reaction explosively generated the formation of orthotitanic acid ($Ti(OH)_4$) to become a titania precursory layer on the I_2 nanoparticles [23]. These primary TiO_2 precursors formed as a shell on the surface of I_2 particles. In other words, the I_2 particles appear as nucleation sites for TiO_2 spheres via the hydrolysis of $TiCl_4$. At room temperature, the hydrolysis of $TiCl_4$ is relatively slow. When the starting solution was heated in an isothermal water bath of 40°C for 2 h and add ammonia solution, it became supersaturated

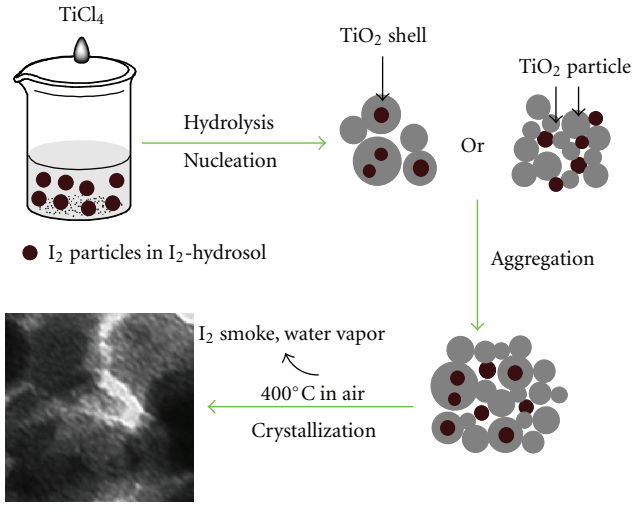

FIGURE 4: Proposed formation mechanism of $(I_2)_n$ sensitized nanoporous TiO_2.

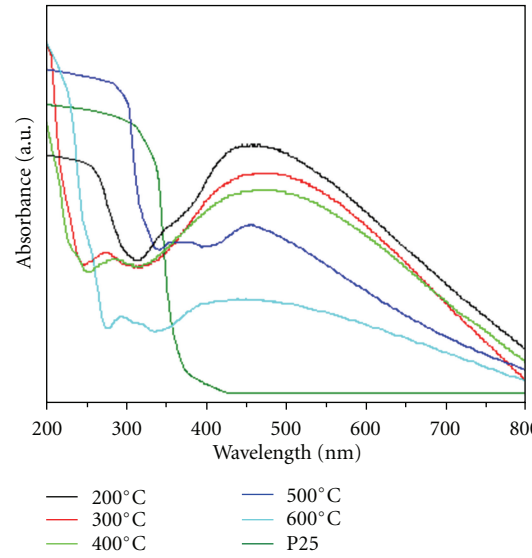

FIGURE 5: UV-vis diffuse reflectance spectra of IT-T catalysts at various calcination temperatures compared to P25.

and precipitated. After drying the precursor turn into $(I_2)_n$-H_2TiO_3. The subsequent calcinated of the precipitated at elevated temperatures leading to a series of reactions among I_2 and TiO_2 precursors with the presence of O_2. We believe that the $(I_2)_n$-sensitized nanoporous TiO_2 is a product of the following synergetic processes, including (1) the I_2 sublimes and the thermal decomposition H_2TiO_3 resulting gaseous products pulverize the TiO_2 shell, leading to the formation of the primary pores. (2) Part of the I_2 attaches to surface of the TiO_2 primary particles. The further oxidation of I_2 is more or less prevented by the shell of primary TiO_2 nanoparticles [7]. (3) The amorphous TiO_2 crystallizes into anatase TiO_2.

3.3. UV-Vis Diffuse Reflectance Spectra. Figure 5 collects the UV-Vis diffuse reflectance spectra of the as-synthesized samples, the P25, as well as the I_2 hydrosol. In comparison to the pure TiO_2, the spectra of $(I_2)_n$ sensitized nanoporous TiO_2 samples exhibit a strong broad absorption band between 400 and 750 nm, covering nearly the entire visible range. This band is centered around 500 nm, which is the spectral range where iodine absorbs [7]. Apparently, the absorbance between 400 and 700 nm decreases for sample prepared at higher temperatures. This can be ascribed to the additional loss of I_2 by sublimation at higher temperatures. But the sample which is obtained at 600°C still has a strong absorption in the visible region. Nonetheless, the absorption in the visible-light region implies that the prepared $(I_2)_n$ sensitized nanoporous TiO_2 samples can be activated by visible light, and that more photogenerated electrons and holes can be created and they can participate in the photocatalytic oxidation reactions. We believe that, with the increase of the temperature during heat treatment, the concentration of iodine molecules on the surface of the IT samples decreased due to sublimation of I_2 at high temperature, which is also confirmed by the color change of the samples during the heat treatment. The color of the samples changed from puce, to brown, slight brown and fawn, and finally to light gray when the temperature increased from 200 to 600°C.

3.4. Photocatalytic Activity on the Decomposition of Methylene Blue. Methylene blue (MB) is a brightly colored blue cationic thiazine dye and is often used as a test model pollutant in semiconductor photocatalysis. A blank experiment was also carried out. The pure MB solution cannot decompose without catalyst. Figure 6(a) shows the adsorption and photodegradation ability on MB solutions of our IT-T samples in comparison to P25. Prior to the turn-on of the light, the concentrations of MB in the presence of the IT-T samples deplete much faster than P25. This is especially seen for IT-200 sample; nearly 70% of the dye molecules were adsorbed within 30 min. We ascribe this effect to the much larger surface area of the IT-T samples than that of P25 as characterized and discussed above. For IT-T samples, their adsorption capacity increases with the decrease of the calcination temperatures. This can be credited to the reduced surface area.

Furthermore, Figure 6(a) shows, under visible light illumination, the MB solutions containing the IT-T samples underwent significant degradation and became nearly transparent within 50 min. In contrast, the MB solutions containing P25 show very limited degradation. It should be noted that IT-400 sample showed the highest photocatalytic oxidation on methylene blue. This is because the crystalline of IT-400 is well and has fewer defects, so the recombination of electron and hole is very low. In addition, the sample still has larger surface area, so IT-400 has good absorption capacity.

The photocatalytic activity of the powders can be quantitatively evaluated by comparing the apparent reaction rate

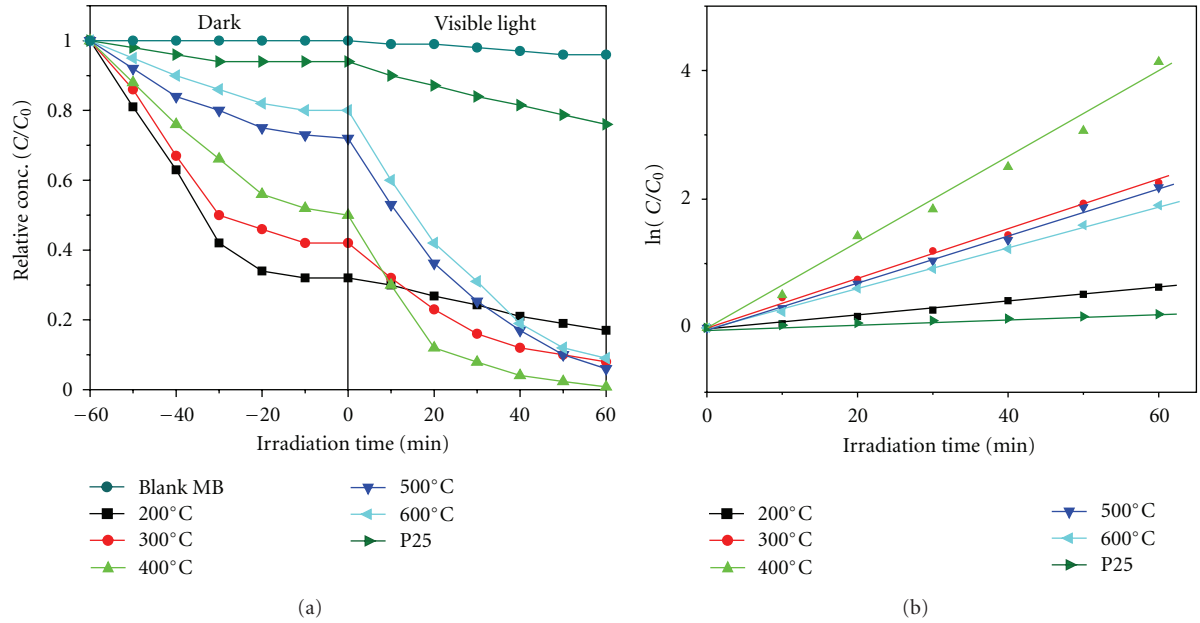

Figure 6: (a) The blank MB solution, photodegradation of methylene blue solutions by using IT-T and P25 under visible light in a neutral suspension. (b) The variation of normalized $\ln(C_0/C)$ of MB concentration as a function of visible light irradiation time.

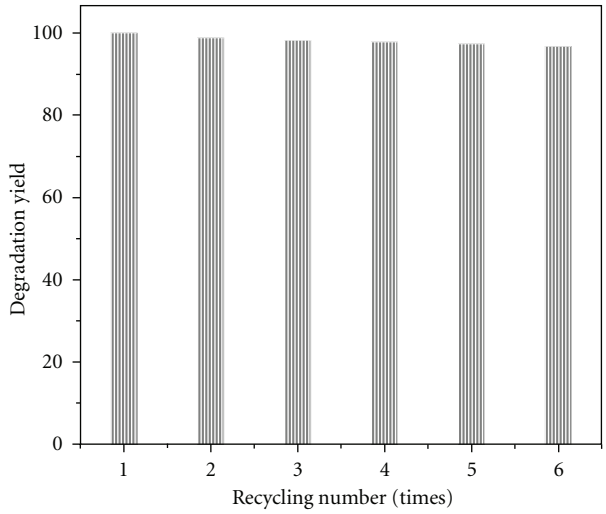

Figure 7: Recycling test result by using the IT-400 sample.

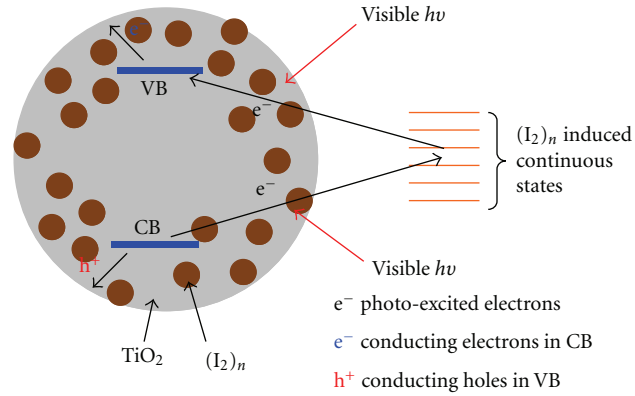

Figure 8: Proposed visible light-driven photocatalytic mechanism on the $(I_2)_n$ sensitized nanoporous TiO_2 nanoparticle.

constants. It is well known that photocatalytic oxidation of organic pollutants in aqueous suspension follows the Langmuir-Hinshelwood model [25], and it can be described as follows [26]:

$$\ln\left(\frac{C_0}{C_t}\right) = k_{\text{app}} \times t, \tag{1}$$

where C_t is the concentration of MB aqueous at reaction time t, C_0 is the initial MB concentration, k_{app} is apparent rate constant, and t is reaction time. The variations in $\ln(C_0/C)$ as a function of irradiation time are given in Figure 6(b). Since all the curves can be fitted roughly to a straight line, the photocatalytic degradation reaction can be assumed to follow first-order kinetics [27]. The rate constant for the photodegradation of the MB using IT-400 is 21 times higher than that of P25. All together, we can conclude that IT-T samples exhibited a strong photocatalytic activity for decomposition of MB under visible light irradiation.

The cyclic stability test under the same conditions of IT-400 sample was also examined and shows excellent photocatalytic activity in degrading MB solution, as shown in Figure 7. No significant decrease in its photocatalytic oxidation activity is observed after being used 6 times, which makes it very promising for practical application.

3.5. Proposed Mechanism for the Enhanced Photocatalytic Activity. The enhanced photocatalytic oxidation activity in IT-T samples is a product of several factors. (1) The

sensitized of $(I_2)_n$ introduces continuous states residing in between the VB and CB of TiO_2 [28]. As schematically elucidated in Figure 8, we believe these I-induced continuous states can either accept visible light-excited electrons from the VB of TiO_2 and/or provide visible-light excited electrons from these I_2-induced states to the CB of TiO_2. (2) Due to the nature of our preparing method, the sensitized I_2 must be preferentially located in the surface region of the TiO_2 nanoparticles. Consequently, the I-induced defective states are preferentially concentrated in the surface region instead of the bulk of the TiO_2, which facilitate the trap of hot carrier in the surface region where the desired photodegradation reactions occur [6, 29]. (3) Because the photo-degradation occurs at the surface of TiO_2, the organic pollute molecules must be preconcentrated at the TiO_2 surface in order to react with the trap hot carriers and the reactive radicals. Thus, the high surface areas of the nanoporous TiO_2 enhance the adsorption of methylene blue molecules onto the surface of TiO_2 particles. This is evidenced by the pronounced more and faster deletion of methylene blue molecules in solution under darkness (Figure 6(a)) in comparison to P25 sample. In addition, large surface area can accommodate more surface-adsorbed water and hydroxyl groups that act as photoexcited hole traps and produce hydroxyl radicals for the degradation of organic pollute molecules [30].

4. Conclusions

In summary, a unique template-free synthetic strategy is used to prepare $(I_2)_n$ sensitized nanoporous TiO_2 through a hydrolysis-calcination process. I_2 hydrosol is used as nucleation center and sensitizer, while the $TiCl_4$ was used as the precursor for TiO_2. The calcination temperature has a crucial role in the amount of $(I_2)_n$ sensitized nanoporous TiO_2. The calcination enhanced the phase transformation of the TiO_2 powders form amorphous to anatase phases and crystallization of anatase. The photocatalytic activity of the as-prepared samples was higher than that of P25 for the degradation of MB. The sample calcined at 400°C shows the highest photocatalytic activity in the decomposition of methylene blue under visible light due to the enhanced absorption in visible region and the large specific surface area.

Acknowledgments

S. Gao and B. Huang thank the National Basic Research Program of China (973 Program, no. 2007CB613302), Doctoral Foundation of Shandong Province (2007BS04040), and Project of Shandong Province Higher Educational Science and Technology Program (J10LF02).

References

[1] A. L. Linsebigler, G. Q Lu, and J. T. Yates, "Photocatalysis on TiO_2 surfaces: principles, mechanisms, and selected results," *Chemical Reviews*, vol. 95, no. 3, pp. 735–758, 1995.

[2] J. Zhang, Q. Xu, Z. C. Feng, M. J. Li, and C. Li, "Importance of the relationship between surface phases and photocatalytic activity of TiO_2," *Angewandte Chemie*, vol. 47, no. 9, pp. 1766–1769, 2008.

[3] H. F. Cheng, B. B. Huang, P. Wang et al., "In situ ion exchange synthesis of the novel Ag/AgBr/BiOBr hybrid with highly efficient decontamination of pollutants," *Chemical Communications*, vol. 47, no. 25, pp. 7054–7056, 2011.

[4] H. P. Li, W. Zhang, and W. Pan, "Enhanced photocatalytic activity of electrospun TiO_2 nanofibers with optimal anatase/rutile ratio," *Journal of the American Ceramic Society*, vol. 94, no. 10, pp. 3184–3187, 2011.

[5] X. N. Wang, B. B. Huang, Z. Y. Wang et al., "Synthesis of Anatase TiO_2 tubular structures microcrystallites with a high percentage of {001} facets by a simple one-step hydrothermal template process," *Chemistry*, vol. 16, no. 24, pp. 7106–7109, 2010.

[6] P. Xu, J. Lu, T. Xu, S. M. Gao, B. B. Huang, and Y. Dai, "I_2-hydrosol-seeded growth of $(I_2)_n$-C- codoped meso/nanoporous TiO_2 for visible light-driven photocatalysis," *Journal of Physical Chemistry C*, vol. 114, no. 20, pp. 9510–9517, 2010.

[7] S. Usseglio, A. Damin, D. Scarano, S. Bordiga, A. Zecchina, and C. Lamberti, "$(I_2)_n$ encapsulation inside TiO_2: a way to tune photoactivity in the visible region," *Journal of the American Chemical Society*, vol. 129, no. 10, pp. 2822–2828, 2007.

[8] P. C. Deng, H. Z. Wang, B. W. Sun, L. X. Fan, and L. Li, "Hydrothermal preparation and photocatalytic performance of $(I_2)_n$ Sensitized and I(V) Doped TiO_2 Supported on SiO_2," *Journal of Advanced Oxidation Technologies*, vol. 12, no. 2, pp. 226–230, 2009.

[9] P. Xu, T. Xu, J. Lu et al., "Visible-light-driven photocatalytic S- and C- codoped meso/nanoporous TiO_2," *Energy and Environmental Science*, vol. 3, no. 8, pp. 1128–1134, 2010.

[10] H. X. Li, X. Y. Zhang, Y. N. Huo, and J. Zhu, "Supercritical preparation of a highly active S-doped TiO_2 photocatalyst for methylene blue mineralization," *Environmental Science and Technology*, vol. 41, no. 12, pp. 4410–4414, 2007.

[11] S. Sakthivel and H. Kisch, "Daylight photocatalysis by Carbon-modified Titanium Dioxide," *Angewandte Chemie*, vol. 42, no. 40, pp. 4908–4911, 2003.

[12] G. S. Wu, T. Nishikawa, B. Ohtani, and A. C. Chen, "Synthesis and characterization of carbon-doped TiO_2 nanostructures with enhanced visible light response," *Chemistry of Materials*, vol. 19, no. 18, pp. 4530–4537, 2007.

[13] R. Asahi, T. Morikawa, T. Ohwaki, K. Aoki, and Y. Taga, "Visible-light photocatalysis in nitrogen-doped titanium oxides," *Science*, vol. 293, no. 5528, pp. 269–271, 2001.

[14] J. Wang, D. N. Tafen, J. P. Lewis et al., "Origin of photocatalytic activity of Nitrogen-doped TiO_2 nanobelts," *Journal of the American Chemical Society*, vol. 131, no. 34, pp. 12290–12297, 2009.

[15] Q. Wang, C. C. Chen, W. H. Ma, H. Y. Zhu, and J. C. Zhao, "Pivotal role of fluorine in tuning band structure and visible-light photocatalytic activity of nitrogen-doped TiO_2," *Chemistry*, vol. 15, no. 19, pp. 4765–4769, 2009.

[16] Z. Y. Liu, H. W. Bai, and D. Sun, "Facile fabrication of hierarchical porous TiO_2 hollow microspheres with high photocatalytic activity for water purification," *Applied Catalysis B*, vol. 104, no. 3–4, pp. 234–238, 2011.

[17] Y. Ide, Y. Nakasato, and M. Ogawa, "Molecular recognitive photocatalysis driven by the selective adsorption on layered titanates," *Journal of the American Chemical Society*, vol. 132, no. 10, pp. 3601–3604, 2010.

[18] Y. Shiraishi, N. Saito, and T. Hirai, "Adsorption-driven photocatalytic activity of mesoporous titanium dioxide," *Journal*

of the American Chemical Society, vol. 127, no. 37, pp. 12820–12822, 2005.

[19] P. Raveendran, M. Eswaramoorthy, U. Bindu et al., "Template-free formation of meso-structured anatase TiO_2 with spherical morphology," *Journal of Physical Chemistry C*, vol. 112, no. 50, pp. 20007–20011, 2008.

[20] J. Fang, F. Wang, K. Qian, H. Bao, Z. Q. Jiang, and W. X. Huang, "Bifunctional N-doped mesoporous TiO_2 photocatalysts," *Journal of Physical Chemistry C*, vol. 112, no. 46, pp. 18150–18156, 2008.

[21] C. A. Nolph, D. E. Sievers, S. Kaewgun et al., "Photocatalytic study of polymorphic titania synthesized by ambient condition sol process," *Catalysis Letters*, vol. 117, no. 3–4, pp. 102–106, 2007.

[22] Y. Z. Li, Y. N. Fan, and Y. Chen, "A novel method for preparation of nanocrystalline rutile TiO_2 powders by liquid hydrolysis of $TiCl_4$," *Journal of Materials Chemistry*, vol. 12, no. 5, pp. 1387–1390, 2002.

[23] A. D. Paola, M. Bellardita, R. Ceccato, L. Palmisano, and F. Parrino, "Highly active photocatalytic TiO_2 powders obtained by thermohydrolysis of $TiCl_4$ in water," *Journal of Physical Chemistry C*, vol. 113, no. 34, pp. 15166–15174, 2009.

[24] K. S. W. Singh, D. H. Everett, R. A. W. Haul et al., "Reporting physisorption data for gas/solid systems," *Pure and Applied Chemistry*, vol. 57, no. 4, pp. 603–619, 1985.

[25] C.-H. Wu, H.-W. Chang, and J.-M. Chern, "Basic dye decomposition kinetics in a photocatalytic slurry reactor," *Journal of Hazardous Materials*, vol. 137, no. 1, pp. 336–343, 2006.

[26] J. G. Yu, G. H. Wang, B. Cheng, and M. H. Zhou, "Effects of hydrothermal temperature and time on the photocatalytic activity and microstructures of bimodal mesoporous TiO_2 powders," *Applied Catalysis B*, vol. 69, no. 3–4, pp. 171–180, 2007.

[27] J. M. Wu and T. W. Zhang, "Photodegradation of rhodamine B in water assisted by titania films prepared through a novel procedure," *Journal of Photochemistry and Photobiology A*, vol. 162, no. 1, pp. 171–177, 2004.

[28] S. Tojo, T. Tachikawa, M. Fujitsuka, and T. Majima, "Iodine-doped TiO_2 photocatalysts: correlation between band structure and mechanism," *Journal of Physical Chemistry C*, vol. 112, no. 38, pp. 14948–14954, 2008.

[29] M. R. Hoffmann, S. T. Martin, W. Choi, and D. W. Bahnemann, "Environmental applications of semiconductor photocatalysis," *Chemical Reviews*, vol. 95, no. 1, pp. 69–96, 1995.

[30] V. Subramanian, E. E. Wolf, and P. V. Kamat, "Catalysis with TiO_2/gold nanocomposites. Effect of metal particle size on the fermi level equilibration," *Journal of the American Chemical Society*, vol. 126, no. 15, pp. 4943–4950, 2004.